Journal of Applied Physics

Stacking order reduction in multilayer graphene by inserting nanospacers

Cite as: J. Appl. Phys. **132**, 174305 (2022); https://doi.org/10.1063/5.0103826
Submitted: 17 June 2022 • Accepted: 02 October 2022 • Published Online: 07 November 2022

Zizhao Xu, Taiki Inoue, Yuta Nishina, et al.

AIP Publishing

Journal of Applied Physics ARTICLE scitation.org/journal/jap

Stacking order reduction in multilayer graphene by inserting nanospacers

Cite as: J. Appl. Phys. **132**, 174305 (2022); doi: 10.1063/5.0103826
Submitted: 17 June 2022 · Accepted: 2 October 2022 ·
Published Online: 7 November 2022

Zizhao Xu,[1,a)] Taiki Inoue,[1] Yuta Nishina,[2] and Yoshihiro Kobayashi[1,a)]

AFFILIATIONS

[1]Department of Applied Physics, Graduate School of Engineering, Osaka University, 2-1 Yamadaoka, Suita, Osaka 565-0871, Japan
[2]Research Core for Interdisciplinary Sciences, Okayama University, 3-1-1 Tsushima-naka, Kita-ku, Okayama 700-8530, Japan

[a)]**Authors to whom correspondence should be addressed:** zizhao_xu@ap.eng.osaka-u.ac.jp and kobayashi@ap.eng.osaka-u.ac.jp

ABSTRACT

Toward macroscopic applications of graphene, it is desirable to preserve the superior properties of single-layer graphene in bulk scale. However, the AB-stacking structure is thermodynamically favored for multilayer graphene and causes strong interlayer interactions, resulting in property degradation. A promising approach to prevent the strong interlayer interaction is the staking order reduction of graphene, where the graphene layers are rotated in-plane to form a randomly stacking structure. In this study, we propose a strategy to effectively decrease the stacking order of multilayer graphene by incorporating nanospacers, cellulose nanofibers, or nano-diamonds (NDs) in the formation process of porous graphene sponges. We conducted an ultrahigh temperature treatment at 1500 °C with ethanol vapor for the reduction and structural repair of graphene oxide sponges with different concentrations of the nanospacers. Raman spectroscopy indicated an obvious increase in the random-stacking fraction of graphene by adding the nanospacers. The x-ray diffraction (XRD) analysis revealed that a small amount of the nanospacers induced a remarkable decrease in ordered graphene crystalline size in the stacking direction. It was also confirmed that a layer-number increase during the thermal treatment was suppressed by the nanospacers. The increase in the random-stacking fraction is attributed to the efficient formation of randomly rotated graphene through the ethanol-mediated structural restoration of relatively thin layers induced by the nanospacers. This stacking-order-reduced graphene with bulk scale is expected to be used in macroscopic applications, such as electrode materials and wearable devices.

I. INTRODUCTION

Graphene has attracted wide attention as a two-dimensional (2D) material for its various excellent properties, such as high carrier mobility, electrochemical performance,[1] optical transparency,[2] thermal conductivity,[3] and mechanical strength.[4] Many of these properties are attributed to the unique electronic structure derived from a one-atom-thick honeycomb lattice of single-layer graphene. However, the electrical, mechanical, and other performances were limited by the thinness and small volume of a single-layer graphene flake. Thus, scaling up high-quality graphene toward bulk-scale, which is composed of plenty of graphene flakes,[5] is necessary for practical applications.[6–13]

Considering mass-production compatibility and structure controllability, a promising approach for producing bulk-scale graphene is beginning with graphene oxide (GO) and then reducing it into reduced graphene oxide (rGO). Hydro-thermal or chemical methods are the most common approaches for reduction.[14,15] However, they produce rGO that suffers from a high density of defects, such as vacancy, which was formed during GO production and remained even after reduction. Alternatively, the defect problem can be solved by high-temperature treatment of GO,[16] while it brings about a problem regarding the stacking structure of multilayer graphene. The thermodynamically stable AB-stacked structure[17] is spontaneously formed at high temperatures. This AB-stacked structure causes a strong interlayer interaction between graphene layers and results in the degradation of the superior properties of single-layer graphene. Conversely, theoretical calculations have predicted that randomly stacked graphene, where each layer is vertically stacked and randomly rotated, can preserve the electronic band structure similar to that of single-layer ones.[18] This is due to the smaller interactions between adjacent graphene layers. Compared to AB-stacked graphene, randomly stacked graphene possesses superior properties for maintaining a single-layer-like electronic structure; this has been confirmed in experimental

studies.[19–21] Individual flakes of randomly stacked multilayer graphene demonstrate a carrier mobility of 7×10^4 cm^2/V s.[22] The development of randomly stacked graphene manufacturing methods is essential for the realization of daily applications of graphene.

Due to the unique reaction pathway, the random-stacking structure of graphene is effectively maintained by adding ethanol vapor during the high-temperature treatment of GO.[23] Ethanol vapor at high temperatures generates carbon containing species and reactive oxygen species (hereafter called "ethanol-derived species"), which respectively function as a carbon-supplying source and an etchant for unstable defective structures in GO during the reduction process. Their synergetic effect enables efficient defect healing of GO without causing intense stacking rearrangement. High carrier mobility was achieved by utilizing this reduction method for few-layer rGO on substrates.[24] However, we found that this method faced the following problem: the repairing and formation of randomly stacked structures were limited to the surface region when preparing bulk-scale graphene. Preparing GO with a porous structure before the ethanol-associated ultrahigh temperature process resolved this issue.[25] This rGO with a porous structure was prepared via freeze-drying of GO dispersion and the ethanol-associated thermal treatment. According to the Raman spectra analysis, both the internal and surface regions of graphene reached ~80% of the random-stacking fraction. To further improve the random-stacking fraction of rGO, we conducted a preliminary experiment on adding cellulose nanofiber (CNF) as a nanospacer.[25] This spacer aims to physically prevent the direct layer stacking of graphene. In addition to the formation of the randomly stacked graphene structure, the insertion of the spacer between graphene layers is expected as an effective approach to reduce the interlayer interaction caused by ordered stacking. Also, the accessibility of ethanol-derived species in the samples can be improved during the thermal treatment, which suppresses the formation of AB stacking. Choosing the spacer was based on the fact that CNF has high water solubility and could transform into inert materials at high temperatures without reacting with GO.[26,27] Considering the 2D structure of graphene and the one-dimensional (1D) structure of CNF, this composite sponge can be regarded as a 2D/1D mixed-dimensional heterostructure, where the material property is designed with the combination of different building blocks.[28] The rGO/CNF sample indicated a higher random-stacking fraction than the pure rGO sample. However, the mechanism of stacking order reduction in the multilayer graphene remained unclear. Thus, a systematic study on spacer concentration and the change in stacking structure along the process sequence is necessary for understanding the stacking mechanism and further controlling the stacking order of graphene.

To address this issue, it should be a promising approach to compare the 1D CNF with another kind of nanospacer material having different dimensionality. Nano-diamond (ND), the candidate for another nanospacer material, is a zero-dimension (0D) material attracting wide attention for its potential applications in catalysis,[29] bio-sensor,[30] and so on.[31] The detonation method is widely used in the industrial preparation of ND. It is followed by an oxidation process that removes impurities on the surface.[32–34] ND particles prepared by the detonation method possess a three-layered structure. The inner two layers of ND, a core layer and an intermediate shell layer, are made up of a cubic diamond crystal (sp^3-hybridization) and the partial layer of a fullerene-like shell (sp^2-hybridization),[35] respectively. The surface layer of ND has oxygen-containing groups, and the mentioned oxidation process can enhance hydrophilicity.[34] Because both ND and GO show a negative Zeta charge, a stable mixed dispersion with electrostatic repulsion is expected. In contrast to the 1D structure of CNF, ND is a 0D material with a low aspect ratio, making the formation of the micrometer-scale agglomerates more difficult. Additionally, ND transforms into a carbon nano onion, that is the nested sp^2 carbon shells, at high temperature.[36] The carbon nano onion is inert and does not react with graphene during the thermal treatment. These advantages make ND a promising candidate as a nanospacer for graphene to produce 2D/0D mixed-dimensional heterostructures with a low stacking order.

In this paper, we propose a method of reducing the stacking order in multilayer graphene using nanomaterials with different dimensions as nanospacers. CNFs or NDs with varied concentrations were added to the GO dispersion, which is the precursor of the GO sponge. Raman spectroscopy and x-ray diffraction (XRD) are used to examine the stacking structures of the bulk-scale multilayer graphene sponge. The Raman analysis indicates a remarkable decrease in the stacking order of graphene even with a low concentration spacer. To clarify the role of the spacer in the decrease of the stacking order, especially the functional difference between CNF and ND, the periodic structure in the graphene samples is investigated based on the XRD analysis. Distinct XRD patterns are observed from the graphene samples, and their analyzed results on the crystalline size in the stacking direction, as well as the layer distance, vary systematically according to the concentration of the spacer. The complicated behavior of the stacking order in graphene with the spacer can be understood by the two-component model, which is proposed based on the XRD analysis of the pre-thermal treatment samples. The different behavior for CNF and ND as spacer materials can be explained by the aggregation effects in the samples observed in scanning electron microscopy (SEM) images. Bulk-scale graphene preserving the properties of single-layer graphene 2D/1D and 2D/0D mixed-dimensional heterostructures will pave the way for macroscopic applications, for example, piezoresistive sensor[9,12] for wearable devices as well as electrode materials in battery[7,8] and supercapacitor.[10,11]

II. MATERIALS AND METHODS

A. Preparation of GO, GO/CNF, and GO/ND dispersion

The 1 wt. % GO/water dispersion was prepared from bulk graphite by a modified Hummers' method.[37] The GO flake size was evaluated to be around 10 μm by optical microscopy. The diluted GO dispersion weight percentage was 0.8 wt. %, which was equal to that of the GO/spacer composite samples.

The CNFs were prepared by the TEMPO method and used as received from DKS Co. They featured a high aspect ratio of 4–10 nm in diameter and 1 μm in length. The GO dispersion was blended with CNFs in water.[25] The GO mass fraction of the dispersion was fixed at 0.8 wt. %, while the CNF mass fraction varied between 0.01, 0.02, 0.05, 0.1, and 0.2 wt. %.

The NDs were prepared by the detonation method and used as received from Nippon Kayaku Co. They featured an average of 5 nm in diameter. The GO dispersion was blended with NDs in water. The GO mass fraction of the dispersion was fixed at 0.8 wt. %, while the ND mass fraction varied between 0.01, 0.02, 0.05, 0.1, and 0.2 wt. %.

B. Preparation of GO, GO/CNF, and GO/ND sponges by freeze-drying

A lab-made vacuum drying system was used for the freeze-drying process.[25] To prepare 1 cm^3 cube sponges of GO with or without spacers, the dispersion was poured into an ice tray and then frozen using liquid nitrogen. The tray was installed in the vacuum drying system, and its chamber was pumped for 72 h. Pumping causes the water in the frozen dispersion to sublimate, leaving the network structure as a GO or composite sponge for the following thermal treatment. The sponges of 0.8 wt. % GO, 0.8 wt. % GO mixed with 0.01 wt. % CNF, and 0.8 wt. % GO mixed with 0.01 wt. % ND were used for the XRD analysis without the thermal treatment, respectively labeled as GO, GO/CNF, and GO/ND.

C. Thermal treatment

The GO and composite sponges were thermally treated in ethanol/Ar under ultrahigh temperature conditions for repair and reduction. The ultrahigh temperature process was performed at 1500 °C using a tubular electric furnace (HT1500-50-32P, HEAT TECH Co.). Its chamber was maintained at low pressure via a vacuum pump. During the temperature rise, we introduced 20 SCCM of Ar under a total pressure of 34.7 Pa. After reaching the set temperature, the thermal treatment was conducted by flowing 98 SCCM of Ar and 2 SCCM of ethanol under a total pressure of 133 Pa. The obtained rGO sample from pure GO was called G-0, while those from GO mixed with 0.01, 0.02, 0.05, 0.1, and 0.2 wt. % of CNFs (ND) were named GC-1, GC-2, GC-3, GC-4, and GC-5 (GD-1, GD-2, GD-3, GD-4, and GD-5), respectively. Additionally, a pure GO sponge was prepared by using an infrared radiation furnace (SR1800G-S, THERMO RIKO Co.) at 1800 °C under Ar environment as reported in our previous study[25] and the sample was named as G-1800-Ar and used as a reference.

D. Characterization

The obtained samples were ground in a mortar and characterized by Raman spectroscopy and XRD. Raman spectra were obtained by LabRAM HR-800 UV (Horiba Jobin Yvon) with an excitation laser wavelength of 532 nm, a power of 1 mW, and a spot size of ~0.7 μm. They were obtained at 20 random spots for each sample, and the averaged spectra were used for further analysis. The G′-band is sensitive to the vertically changed structure of the graphene plane. Thus, the volume fraction of the randomly stacked structure can be analyzed by G′-band fitting.[38,39] The G′-band profile is the sum of several peaks originating from both random-stacked and AB-stacked structures.[38] Note that in the literature, the G′-band is also represented as the 2D band.[40] To distinguish this Raman band from two-dimensional (2D), we use the G′-band notation in this paper. Details of the fitting process are described in Sec. III and our previous paper.[25] The XRD measurements for the G-0, GC, and GD series samples were conducted using Ultima IV (Rigaku Co.) via a standard Cu-Kα source having λ = 1.5406 nm, with 40 kV and 40 mA. The accuracy of XRD measurement was confirmed by measuring silicon powders and detecting Si 111 peak at 28.4°. The measurements for the samples without thermal treatments (GO, GO/CNF, and GO/ND) were conducted by SmartLab (Rigaku Co.) using a standard Cu-Kα source of λ = 1.5406 nm, with 40 kV and 40 mA. The scanning speed from 10° to 20° was 0.5°/min. To evaluate the ordered structures of stacked GO and rGO with and without spacers, the XRD patterns were analyzed by Bragg's and Scherrer's equations. SEM images were taken by VE-8800 (Keyence) at an acceleration voltage of 15 kV. Samples before grinding were used for the SEM observation.

III. RESULT AND DISCUSSION

A. Raman analysis of stacked graphene with CNFs

The structure of rGO sponge with CNFs as spacers was evaluated by Raman spectroscopy. The Raman spectra of the GC-1, GC-2, GC-3, GC-4, GC-5, and the control group samples, G-0 and G-1800-Ar, were measured as shown in Fig. 1(a). The G-band was observed at around 1580 cm^{-1}, while the D-band was around 1350 cm^{-1}. The G-band derives from the in-plane stretching mode of the hexagonal lattice of graphene, and the D-band originates from the hexagon-breathing mode activated by the presence of lattice defects.[41] The intensity ratio of the D-band to the G-band, $I(D)/I(G)$, corresponds to the defect density of graphene.[41] Additionally, the G′-band of the samples was observed at around 2700 cm^{-1} with varying peak shape and intensity. Because the G′-band is sensitive to the layer number and stacking order of graphene,[42–44] the intensity ratio of the G′-band to the G-band, $I(G')/I(G)$, provides information related to the interlayer interactions of graphene.

The $I(D)/I(G)$ and $I(G')/I(G)$ ratios of the samples are plotted against the CNF concentration in Fig. 1(b). The $I(D)/I(G)$ ratios of the GC series samples ranged between 0.81 and 0.88, while that of G-0 was 0.57. The relationship between the D-band intensity and the defect density was classified into two different stages depending on the latter, namely, the inter-defect distance.[45] In the case of a distance larger than ~3 nm, the D-band intensity increases with an increase in defect density; this is called stage 1. Whereas in the case of an inter-defect distance less than ~3 nm, the intensity decreases with an increase in defect density; this is named stage 2.[45] Stages 1 and 2 can be distinguished by the broadening of the D-band. Our samples were in stage 1 because the full width at half maximum (FWHM) of the D-band ranged between 60 and 70 cm^{-1}.[46,47] Compared to G-0, GC series samples demonstrated a higher $I(D)/I(G)$ ratio, indicating that they featured a higher defect density. This increase in D-band intensity was attributed to the change in the structural restoration of GO induced by adding CNFs. The $I(D)/I(G)$ ratios of the GC series samples were almost constant while the CNF concentration varied, indicating that amorphous carbon formed by incomplete graphitization of CNF did not strongly influence the increase in D-band intensity.

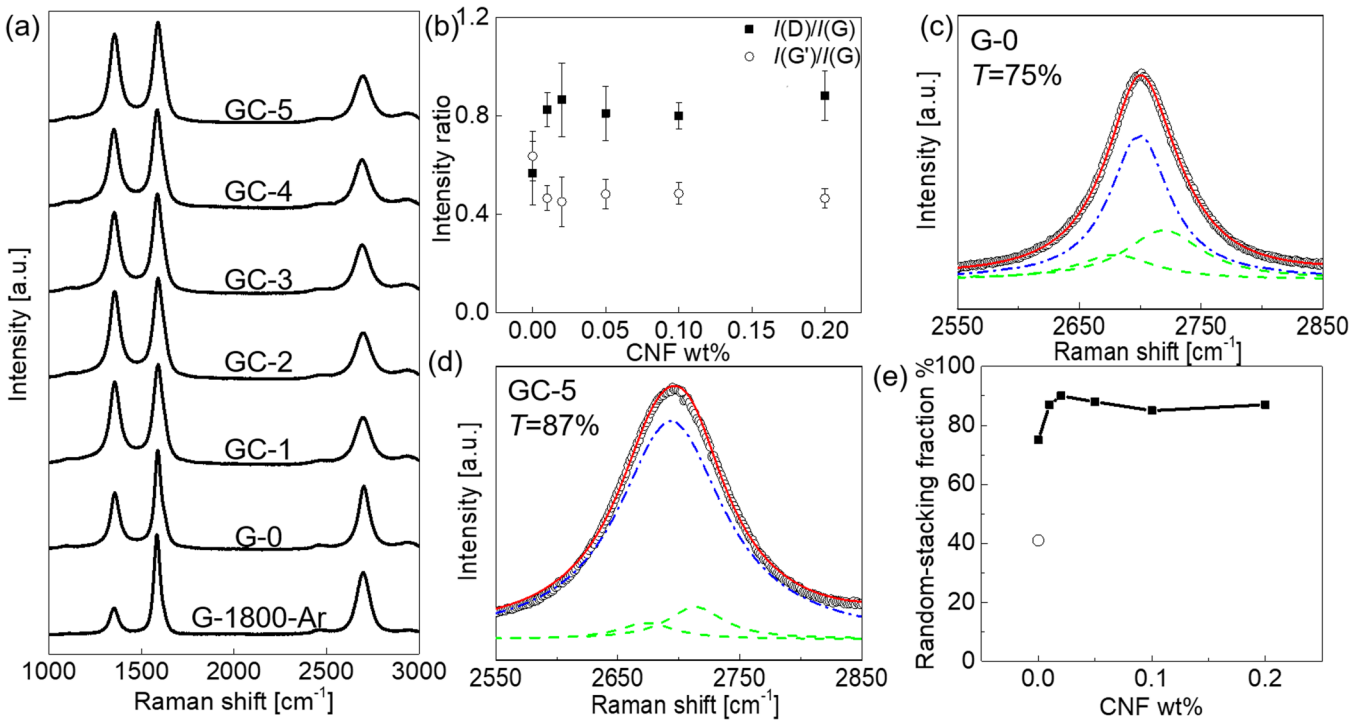

FIG. 1. (a) Raman spectra of the GC series samples, G-0, and G-1800-Ar. (b) Intensity ratios of D-band to G-band, I(D)/I(G), and G′-band to G-band, I(G′)/I(G), plotted against the CNF weight percentage (G-0 and GC series samples). Filled squares denote the I(D)/I(G) ratio, and open circles denote the I(G′)/I(G) ratio. (c) and (d) G′-band fitting of (c) G-0 and (d) GC-5, which provides the randomly stacked structure ratio, T. Black open circles denote the measured spectra. Blue dashed-dotted curves denote the G'_{2D} components originating from the randomly stacked structure of graphene, while the two green dashed curves denote the G'_{3DA} and G'_{3DB} components derived from the AB-stacked structure. Red solid curves are the sum of the blue and green curves. (e) Random-stacking fraction of samples with different weight percentages of CNF. Filled squares denote the random-stacking fraction of the GC series samples and G-0. The open circle denotes that of G-1800-Ar.

The I(G′)/I(G) ratios of the GC series samples (0.45–0.49) were lower than that of G-0 (0.64), and their dependence on the mass fraction of CNF exhibited an opposite trend of I(D)/I(G). This implies that the increase in defects leads to a decrease in the G′-band intensity;[48] thus, the simple comparison of the I(G′)/I(G) ratio is not suitable for evaluating the stacking order of graphene. Actually, the G′-band was observed to shift slightly to a lower frequency by ∼7 cm^{-1} after adding the spacer, corresponding to the increase in the randomly stacking fraction as shown by further analysis of the G′-band described below. To investigate the stacking order of multilayer graphene with CNFs, further analysis on the G′-band was conducted as follows.

As conducted in our previous research, the stacking order of graphene in the bulk-scale samples was evaluated by analyzing the peak shape of the G′-band.[25] According to the research of Cançado *et al.*,[38] the G′-band of multilayer graphene can be deconvoluted using three Lorentzian peaks. The frequency of the first one is close to that of the original G′-band of single-layer graphene, which was located at about 2700 cm^{-1}. According to Ref. 38, this G′-band component is denoted as the G'_{2D} component because it is associated with the 2D graphite feature, which possesses a low stacking order along the c-axis, namely, a turbostratic or randomly stacked structure. The other two peaks are denoted as the G'_{3DA} and G'_{3DB} components, which are located around 2680 and 2720 cm^{-1}, respectively. These are related to the three-dimensional (3D) configuration of graphite, that is, the AB-stacked structure. The G'_{3DB} intensity is in proportion to the 3D graphite volume.[38,49] Cançado's method was employed to calculate the fraction of random-stacking structure in the bulk-scale graphene. From the intensities of the three components, the fraction of random-stacking graphene, T, can be written as

$$T\ [\%] = \frac{I(G'_{2D})}{I(G'_{3DB}) + I(G'_{2D})} \times 100, \quad (1)$$

where $I(G'_{2D})$ and $I(G'_{3DB})$ denote the intensities of G'_{2D} and G'_{3DB} peaks, respectively. For an ideal random-stacking structure of multilayer graphene, the Raman spectrum demonstrates single-layer graphene-like features, i.e., a strong G'_{2D} peak with negligible G'_{3DA} and G'_{3DB} ones, which will result in a T value close to 100%. Note that Mohapatra *et al.*[50] provided a new method based on the strong and constant intensity of I(G′) for graphene with 100% randomly stacking fraction. This method should be very reliable for defect-free graphene; however, it is not suitable for our research using defective graphene as samples because the I(G′) decreases for

the increasing defects,[51] leading to overestimating the volume of the AB-stacking structure.

Via the stacking order analysis based on the G′-band shape, the control group sample, G-1800-Ar, showed a low T value of 40%,[25] as shown in the supplementary material, Fig. S3. This result indicates the preferential formation of a thermodynamically stable AB-stacking structure at high temperatures without the introduction of ethanol. Another control group, G-0, showed a moderate T value of 75% [Fig. 3(c)], which confirms the ethanol effect on suppressing the formation of AB-stacking structure.[23,25,52] By adding CNFs, GC-5 showed a T value of 87% [Fig. 3(d)], which is higher than that of the spacer-less graphene sample, G-0, obtained with an identical high-temperature treatment. Other GC samples (GC-1, GC-2, GC-3, and GC-4) also displayed similar T values, ranging between 85% and 90% [Fig. 3(e)]. This concluded that the majority of the graphene structures of the GC samples were constructed from randomly stacking layers. The T values of GC series samples did not greatly differ when the CNF concentration increased, which requires further analysis to understand the mechanism of determining random-stacking fractions. Note that although the stacking order can be featured by the G′-band analysis, the thickness of multilayer graphene that composes the sponges remains unknown using the Raman spectra. Thus, the evaluation of graphene stacking order using XRD analysis will be given in Sec. III C.

B. Raman analysis of stacked graphene with NDs

Since the ND particles possess a smaller diameter and lower dimensionality than those of CNF, a more effective insertion of ND is expected. Therefore, we attempted to improve the T value of graphene by changing the spacer material to ND. The Raman spectra of GD-1, GD-2, GD-3, GD-4, and GD-5 were measured and plotted with the control groups, G-0, and G-1800-Ar, in Fig. 2(a). The G-band was observed to be around 1580 cm^{-1}, while the D-band was around 1350 cm^{-1}. The I(D)/I(G) ratios of the GD series samples ranged between 0.42 and 0.65 [Fig. 2(b)]. Our samples were on stage 1 because the FWHMs of the D-bands ranged between 50 and 90 cm^{-1}.[46,47] The G′-band of the samples was observed to be around 2700 cm^{-1} with varying peak shape and intensity. The I(G′)/I(G) ratios of GD series samples ranged between 0.45 and 0.72.

The G-0 and GD series samples demonstrated similar I(D)/I(G) and I(G′)/I(G) ratios with small fluctuations, indicating that the GD series samples featured a comparably low defect density

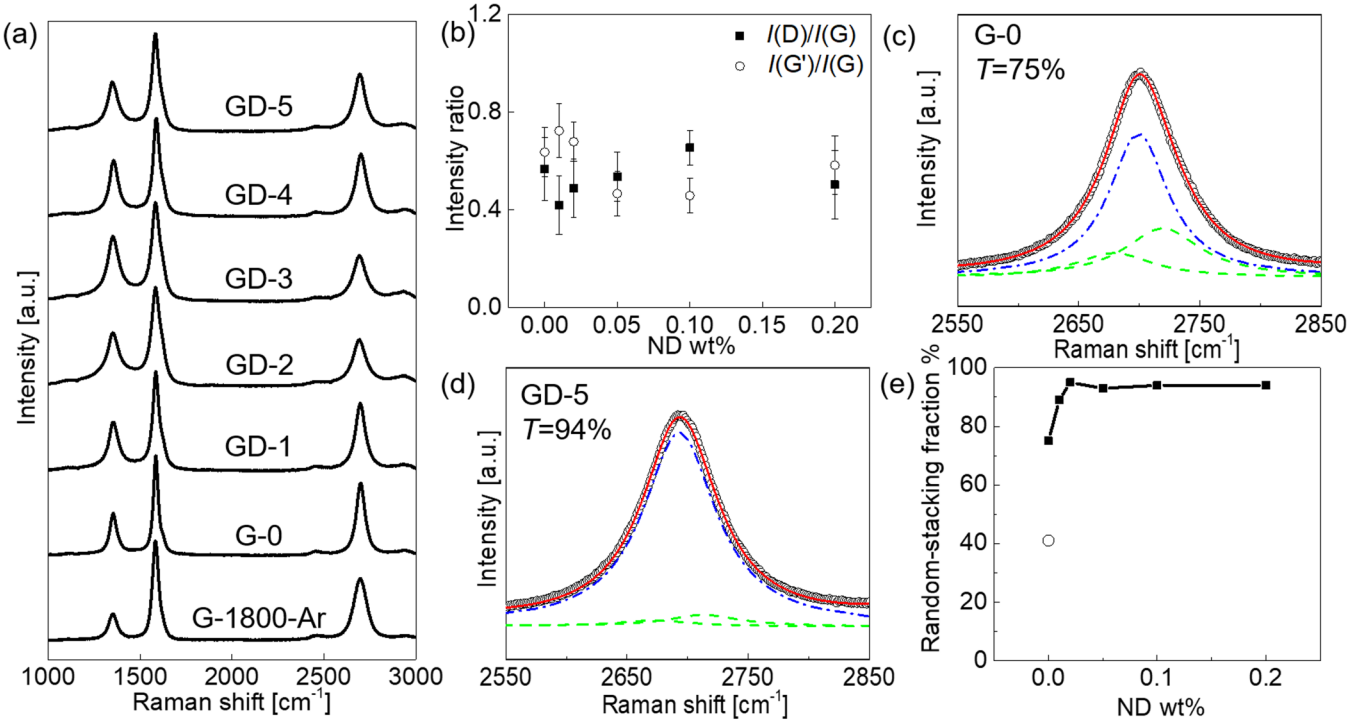

FIG. 2. (a) Raman spectra of the GD series samples, G-0, and G-1800-Ar. (b) The intensity ratios of D-band to G-band, I(D)/I(G), and G′-band to G-band, I(G′)/I(G), plotted against the ND weight percentage (G-0 and GD series samples). Filled squares denote the I(D)/I(G) ratio, and open circles denote the I(G′)/I(G) ratio. (c) and (d) G′-band fitting of (c) G-0, the same as in Fig. 1(c), and (d) GD-5, which provides the randomly stacked structure ratio, T. Black open circles denote the measured spectra. Blue dashed-dotted curves denote the G'_{2D} components originating from the randomly stacked structure of graphene, while the two green dashed curves denote the G'_{3DA} and G'_{3DB} components derived from the AB-stacked structure. Red solid curves are the sum of the blue and green curves. (e) Random-stacking fraction of samples with different weight percentages of ND. Filled squares denote the random-stacking fraction of the GD series samples and G-0. The open circle denotes that of G-1800-Ar.

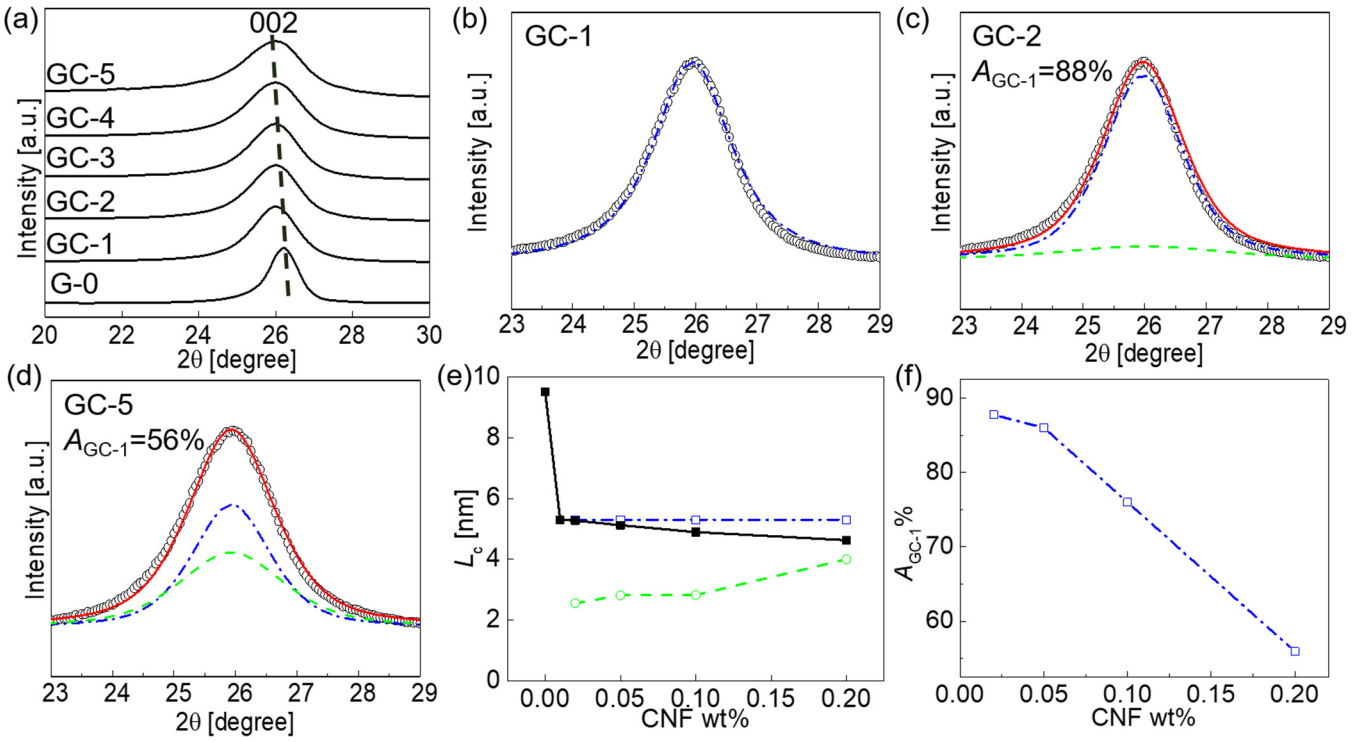

FIG. 3. (a) XRD patterns of the GC series samples and G-0. The 002 peaks of graphene are observed at ~26°. (b) Fitting of the GC-1 002 peaks. Black open circles denote the measured XRD patterns. Blue dashed-dotted curves denote the fitting curve with a single pseudo-Voigt function. (c) and (d) Deconvolution of the 002 peaks of (c) GC-2 and (d) GC-5 into two components. Black open circles denote the measured XRD patterns. Blue dashed-dotted curves denote the first components originating from the stacked structure of graphene possessing the same d_{002} and L_c as GC-1, while the green dashed curves denote the second components derived from the one possessing the same d_{002} as GC-1 but smaller L_c. Red solid curves are the sum of the blue and green one. Ratios of the first component areas over the total peak area, A_{GC-1}, are displayed. (e) L_c of different CNF concentration samples (filled black squares, G-0, and GC series samples). Blue open squares with dashed-dotted lines denote the L_c of the first components, while green open circles with dashed lines denote the second components. (f) A_{GC-1} plotted against the CNF weight percentage.

with G-0. This similar D-band intensity indicated that NDs did not significantly hinder the reduction process nor transform into substances that show a strong D-band. Similarly to the GCs, a slight decrease in the G′-band frequency for the GD samples was observed, after adding the spacer. To understand the stacking order, further analysis on the G′-band was conducted as follows.

Via the stacking order analysis based on the G′-band shape,[38] GD-5 showed a T value of 94% [Fig. 3(d)], which is higher than that of the spacer-less graphene sample, G-0. Other GD samples (GD-1, GD-2, GD-3, and GD-4) also displayed high T values ranging between 89% and 95% [Fig. 3(e)]. Similar to the GC samples, this result concluded that most of the GD samples were constructed from the graphene layers with randomly stacking structures. Compared to that of the GC series samples, the GD ones showed an even higher T value. This indicates that NDs should be highly effective compared with CNFs when it comes to decreasing the stacking order of multilayer graphene. The T values of the GD samples did not differ largely when the ND concentration increased. The details of the stacking structure variations will be further discussed by combining the result of the XRD analysis in Sec. III D.

C. X-ray diffraction analysis of stacked graphene with CNFs

Figure 3(a) shows the XRD patterns measured from the CNF-incorporated rGO sponges (GC series) and pure rGO sponge (G-0). The 002 peak derives from the periodicity of the graphene layer in the stacking direction. The 002 peak position indicates the layer distance of the samples, while the FWHM of the 002 peak corresponds to the crystalline size in the stacking direction. The 002 peak position of G-0 was at 26.2°, and its FWHM was 0.85°. These values were obtained by fitting the peak with a pseudo-Voigt function, which is commonly used for XRD analysis of graphite.[50] The peak positions and the FWHM of the 002 peaks from the GC series samples ranged between 25.9°–26.0° and 1.52°–1.74°, respectively.

The layer distances (d_{002}) of the GC series samples and G-0 were calculated by Bragg's equation,

$$d = \frac{n\lambda}{2\sin\theta}, \tag{2}$$

where n, d, θ, and λ denote the diffraction order, the layer distance, the glancing angle, and the wavelength, respectively. The results

showed that d_{002} of G-0 was 0.340 nm, while that of GC-1, GC-2, GC-3, GC-4, and GC-5 ranged between 0.342 and 0.343 nm. Compared to G-0, GC samples showed larger layer distances in the stacking direction, indicating that the addition of CNFs enlarged the layer distance of stacked graphene. This slight increase indicates a decrease in the layer number of graphene; this is because the layer number and distance are directly correlated.[53] Note that d_{002} of bulk graphite is 0.335 nm,[54,55] while that of a typically stacked rGO is about 0.341 nm.[56] The details of the layer number will be discussed later.

The crystalline sizes (L_c) of the GC series samples and G-0 analyzed from the XRD patterns were shown in Fig. 3(e). The L_c was determined by Scherrer's equation as follows:

$$L_c = \frac{K\lambda}{\beta \cos\theta}, \tag{3}$$

where K denotes the shape factor, which was 0.9;[57] β, θ, and λ denote the FWHM of the 002 peak, the glancing angle, and the wavelength, respectively. Applicability of Scherrer's equation is 3–100 nm.[58] The L_c values analyzed from XRD for G-0 and GC samples were 9.50 nm and 4.63–5.29 nm, indicating the suitability of Scherrer's equation to these samples. By adding CNFs as a spacer material, L_c decreased with an increase in CNF concentration. This was particularly clear in the comparison between G-0 and GC-1. Even when a little amount of CNF (actually, the smallest in this experiment) was added, the fraction of the random-stacking structure significantly increased from 75% to about 85% [Fig. 1(e)], whereas L_c rapidly decreased from 9.50 to 5.29 nm. This indicates that CNFs contribute to the crystalline size reduction due to their role as a spacer between layers. By dividing L_c by d_{002}, a characteristic layer number of stacked graphene, which is active for XRD measurement, can be obtained. The characteristic layer number of G-0 and GC-1 was calculated to be about 28 and 15 layers, respectively, indicating that the stacking of graphene layers is suppressed by the addition of CNFs.

It should be mentioned that the 002 peak fitting with only a single pseudo-Voigt function resulted in a relatively high residential error of 18%–25% for GC-2 to GC-5, while G-0 and GC-1 displayed a low error of 13% and 16%, respectively, as shown in the supplementary material, Fig. S6(a). The large errors indicate that the high CNF concentration samples have large structural variation and cannot be represented by a single component of periodically stacked graphene. Considering the drastic decrease of L_c with a small number of CNFs and its following gradual decrease with the increase in CNFs, it is expected that the spacer will first separate stacked graphene into thin components and then make them even thinner with an increase in CNF concentration. Thus, for simplicity of the analysis, we assume that stacked graphene can be mainly classified into two components, namely, the first and the second ones. The first component is regarded as the main component formed by adding a small number of CNFs, and the second component is formed by increasing the CNF fraction. We conducted the peak fitting of the 002 peak with two pseudo-Voigt functions as described in detail later and found that the residential error of GC-2 to GC-5 was significantly reduced to 9%–13%, as shown in the supplementary material, Fig. S6(a). This confirms the effectiveness of the two peak deconvolution and the validity of the assumption.

Since all GC series samples showed a 002 peak at similar 2θ angles, we considered that the first and second components of each sample maintained the same layer distance. Thus, both 2θ angles of the first and second components were fixed to their original values obtained by the single component fitting. The FWHM of the first component was fixed to that of GC-1 such that its L_c was identical to that of GC-1. To evaluate the relative abundance of the first component, $A_{GC\text{-}1}$ was obtained by taking the ratio of its area over the total peak area.

This analysis was applied for the XRD patterns of the GC series samples, except for GC-1. The fitting results are shown in Figs. 3(c) and 3(d) and in the supplementary material. $A_{GC\text{-}1}$ decreased from 88% to 56% for GC-2 and GC-5, respectively. The change in L_c of the second component and $A_{GC\text{-}1}$ are shown in Figs. 3(e) and 3(f), respectively. This tendency indicates that by increasing the CNF concentration, the formation of the first component was restrained, while that of the second was enhanced. It should be noticed that Raman signals reflect whole portions of samples, and the analysis of G′-band indicates that the fraction of randomly stacking graphene is almost constant for the samples with the addition of the spacer, as shown in Figs. 1(e) and 2(e). This result should allow us to assume that both the first and the second components possess the same fraction of the randomly stacking graphene.

Based on the XRD fitting results, we can infer that the stacking process of graphene with the addition of CNFs can be regarded as a two-step process. In the first one, the GO aggregates to the first component size, and the low concentration of CNF restrains the further aggregation between the first components, leading to a decreased L_c of GC-1, which is about half of that of G-0. As a result, the accessible region for the ethanol-derived species, where the formation of AB-stacking is suppressed, is increased, explaining why the T value of GC-1 increases compared to that of G-0. If the spacer concentration is high, the second step will occur simultaneously. In this process, the spacer physically restrains the formation of the first component, especially in high CNF concentrations. The GO flakes are formed into the second component with fewer layers. Therefore, the CNF concentration strongly affects the second component fraction.

D. X-ray diffraction analysis of stacked graphene with NDs

The XRD patterns of the GD sponges and G-0 as the control group are shown in Fig. 4(a). The 002 peak positions of the GD sponges ranged between 25.9° and 26.0°. The FWHM of the peaks ranged from 1.27° to 1.82°. During fitting, we also found that the residential error of GD-2 to GD-5 could be reduced from 10%–15% to 7%–10% by using the two-peak fitting in a similar manner to the one used with the GC samples [Fig. S6(b) in the supplementary material].

Using Bragg's equation (2), the calculated d_{002} values of GD-1, GD-2, GD-3, GD-4, and GD-5 ranged between 0.342 and 0.344 nm. Compared to G-0, GD samples showed a larger layer distance in the stacking direction. The observed expansion of d_{002}

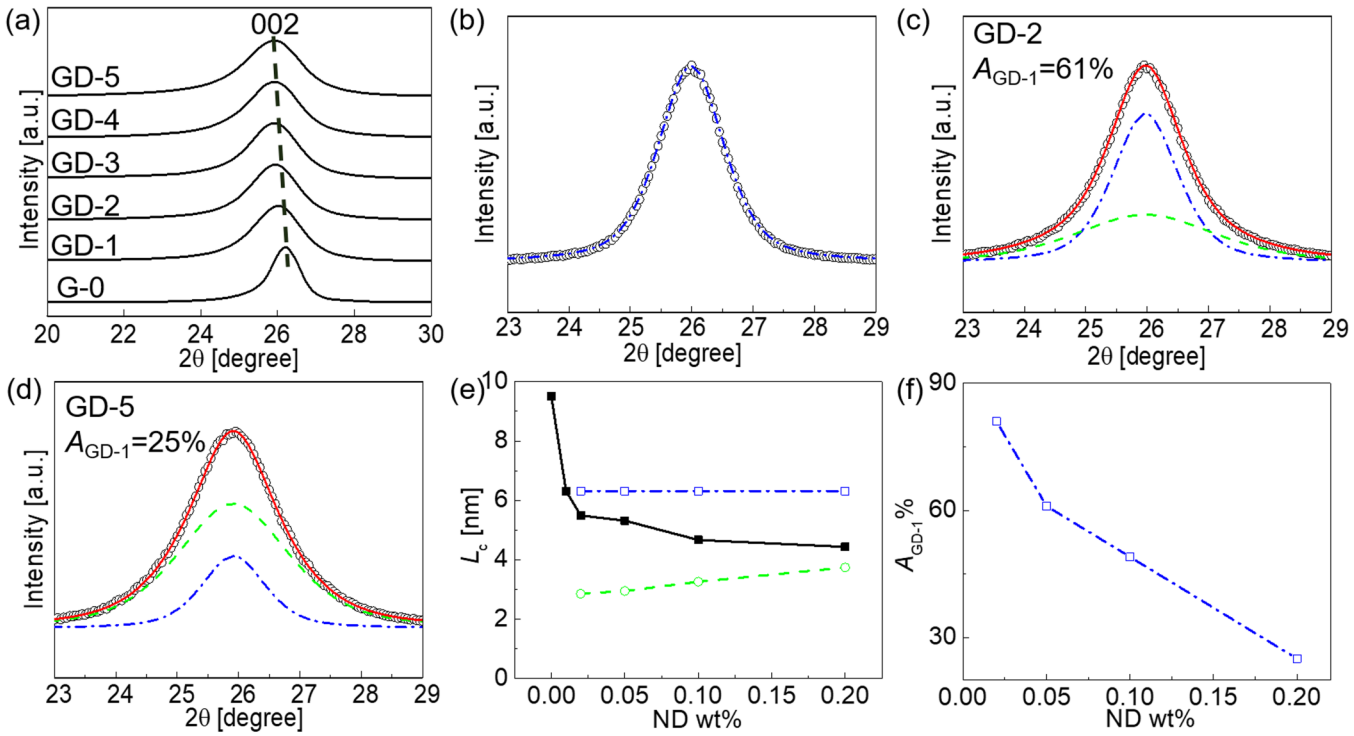

FIG. 4. (a) XRD patterns of the GD series samples and G-0. The 002 peaks of graphene are observed at ~26°. (b) Fitting of the GD-1 002 peaks. Black open circles denote the measured XRD patterns. Blue dashed-dotted curves denote the fitting curve with a single pseudo-Voigt function. (c) and (d) Deconvolution of the 002 peaks of (c) GD-2 and (d) GD-5 into two components. Black open circles denote the measured XRD patterns. Blue dashed-dotted curves denote the first components originating from the stacked structure of graphene possessing the same d_{002} and L_c as GD-1, while the green dashed curves denote the second components derived from the stacked structure of graphene possessing the same d_{002} as GD-1 but smaller L_c. Red solid curves are the sum of the blue and green ones. The ratios of the first component areas over the total peak area, A_{GD-1}, are displayed. (e) L_c of different ND concentration samples (filled black squares, G-0, and GD series samples). Blue open squares with dashed-dotted lines denote the L_c of the first components, while the green open circles with dashed lines denote the second components. (f) A_{GD-1} plotted against the ND weight percentage.

implies that ND decreased the layer number since graphene with smaller layer numbers had a larger layer distance.[53]

By adding NDs as a spacer material, L_c decreased with an increase in ND concentration [Fig. 4(e)]. The L_c[58] of the GD samples ranged 4.43–6.31 nm. This was particularly manifest in the comparison between G-0 and GD-1. When the smallest amount of NDs was added, the fraction of the random-stacking structure increased significantly from 75% to around 95% [Fig. 2(d)], whereas L_c rapidly fell from 9.50 to 6.31 nm. This indicates that NDs contribute to the size reduction of ordered structures of stacked graphene, presumably due to their function as spacers between layers. By dividing L_c by d_{002}, the characteristic layer number of the GD samples was calculated to be around 18 layers.

The analysis method based on two components was applied for the XRD patterns of the GD series samples, except for GD-1. After fitting, the area fraction of the first component, A_{GD-1}, was obtained using the ratio of the first component area to the total peak area. The fitting results are shown in Figs. 4(c) and 4(d) and Fig. S5 in the supplementary material. The first component fraction, A_{GD-1}, decreased from 81% to 25% for GD-2 and GD-5, respectively. The change in L_c of the second component and A_{GC-1} are shown in Figs. 4(e) and 4(f), respectively. This tendency indicates that by increasing the ND concentration, the formation of the first component was restrained, while the second component was enhanced.

The fitting results of XRD indicate that the process of the stacking order change in the ND-incorporated samples can be understood similarly to the case of CNFs, which was described in Sec. III C. In addition, compared with GC samples, GD ones demonstrated a low A_{GD-1}, indicating that GD possessed a higher efficiency in restraining the formation of the first component. The reason for the decreased restraining efficiency of CNF will be discussed in Sec. III E.

It should be mentioned that XRD and Raman spectroscopy provides information on different portion of samples. Since diffraction occurs only from periodic structures of samples, XRD can evaluate crystalline structures but cannot detect un-periodic structures, including amorphous structures and graphene separated by spacers. On the other hand, Raman signals reflect whole portions of samples in each measurement spot. Note that the smaller

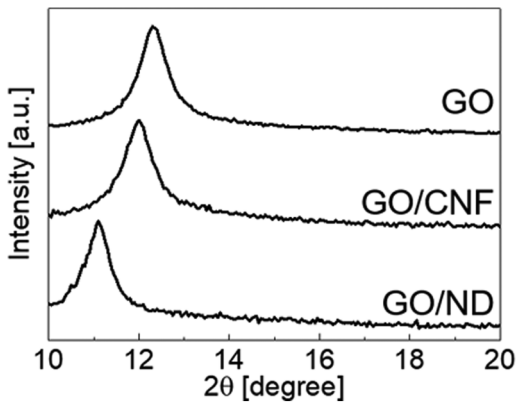

FIG. 5. XRD patterns of GO, GO/CNF, and GO/ND.

measurement area of Raman spectroscopy was compensated by the measurement at multiple spots. We characterized the random stacking ratio of whole samples by Raman spectroscopy and utilized XRD for the deep analysis of relatively thick periodic portions of samples, including AB-stacked graphene whose formation should be suppressed. This evaluation scheme is effective for investigating the stacking order of bulk scale graphene. Selected area electron diffraction (SAED) provides the direct information on the structure of turbostratic graphene, such as twist angle.[59] However, SAED is not capable of measuring our sample, three-dimensional graphene sponge, since SAED can only be utilized for a thin sample. We would prepare graphene thin film with twisted stacking and adequate thickness for SAED observation in future research.

E. Mechanism of stacking order change with nanospacers

By comparing G-0 with GC-1 and GD-1, we found that L_c decreased to almost half after adding spacers. To find out in which process the change in stacking happened, we conducted XRD measurements of the sponge samples before thermal treatment (GO, GO/CNF, and GO/ND). Figure 5 shows the XRD pattern observed from the sponge prepared by freeze-drying the dispersions of the GO, GO/CNF, and GO/ND, in which the 002 peaks were located at 12.3°, 12.0°, and 11.1°, and their FWHM were evaluated to be 0.75°, 0.75°, and 0.63°. The 002 peaks from GO/CNF and GO/ND shifted to lower angles, compared to that of GO. These shifts should be caused by the difference in the pH values for the dispersions.[60] The pH values for the dispersions of GO, GO/CNF, and GO/ND measured before freeze-drying were 2.6, 2.9, and 3.5. The oxygen functional groups on the GO flakes showed increased repulsion due to the negative charge with an increase in pH,[60] leading to the larger layer distance for a higher pH value. The d_{002} and L_c can be evaluated by applying Bragg's and Scherrer's equations, (2) and (3), with the observed FWHM and 002 peak angles. Obtained values of the d_{002} for GO, GO/CNF, and GO/ND were 0.72, 0.74, and 0.80 nm, and those of L_c[58] were 10.55, 10.62, and 12.45 nm. The d_{002} of the pre-thermal treatment samples was larger than that of the corresponding ones with thermal treatment due to the oxygen-containing groups in GO.[61]

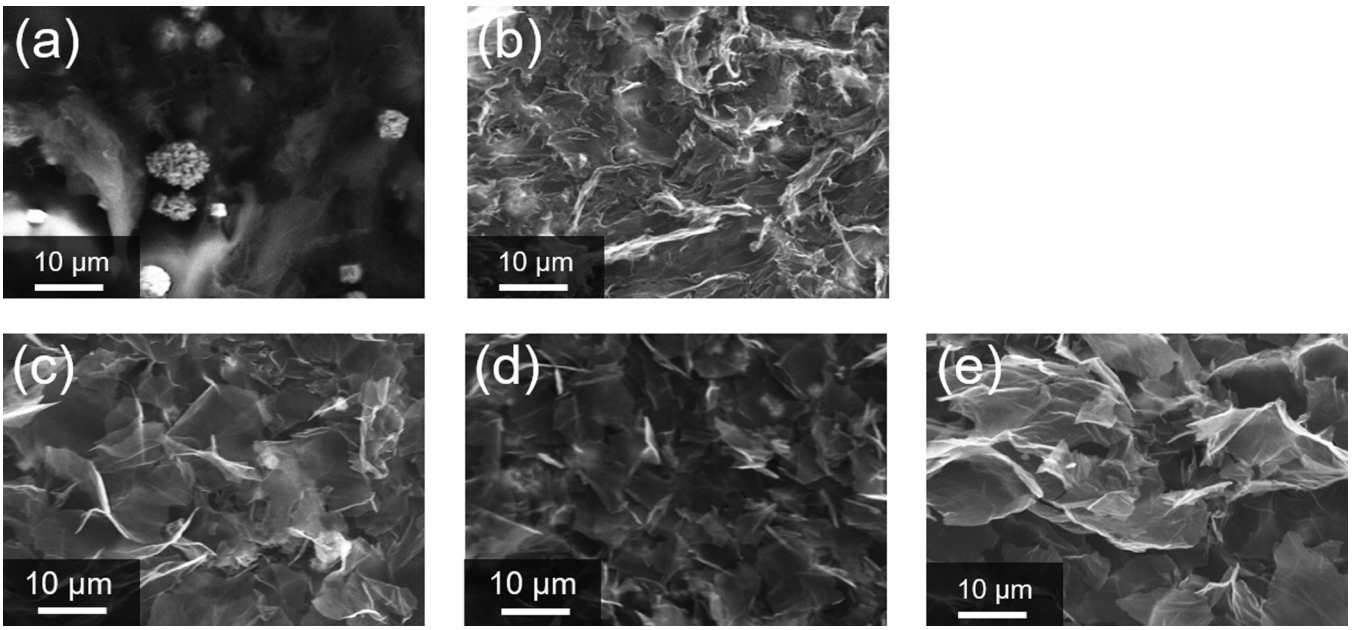

FIG. 6. SEM images of (a) GC-5, (b) GC-1, (c) GD-5, (d) GD-1, and (e) G-0.

From d_{002} and L_c, the characteristic layer numbers of these samples were calculated as ~14, 15, and 16 layers, respectively. This indicates that the stacking number of GO layers before the thermal treatment does not significantly differ even after adding spacers. The layer number is comparable to that of the GC (~15) and GD (~18) series samples but is about half of that of G-0 (~28). Thus, we can infer that in the case without spacers, the layer number of stacked graphene increased during the thermal treatment probably due to the merge of the stacked GO units originally separated by void gaps. In contrast, the layer number was preserved during the thermal process in the case of the spacer addition. This represents the role of the spacers in suppressing the graphene stacking during the thermal treatment by physically separating the stacked GO units.

SEM images of the GC-5, GC-1, GD-5, GD-1, and G-0 showed porous structures of graphene sponges (Fig. 6), confirming that freeze-drying successfully formed a high surface-area structure preserved even after the thermal treatments at high temperature. Particles of around 10 μm in size were observed on GC-5 [Fig. 6(a)], while none were to be seen on GC-1, GD-5, GD-1, and G-0 [Figs. 6(b)–6(e)]. This indicates that part of the CNF was aggregated into the particles in high concentration, obstructing it from playing a spacer role in the GO composite. Thus, the CNF results in less contribution to the stacking order reduction in the following process at high concentration. On the other hand, no ND aggregate was observed, indicating that ND continued to work as a spacer even in high concentrations.

Based on the results and the above discussion, we summarized the stacking order reduction mechanism in multilayer graphene by inserting nanospacers in Fig. 7. The change in stacking order is divided into three stages and three steps depending on the concentration of spacers and the process. In the first stage (Fig. 7, left), without adding any spaces at step (i), the pure graphene sponge showed a large L_c of 9.50 nm and a relatively low T value of 75%.

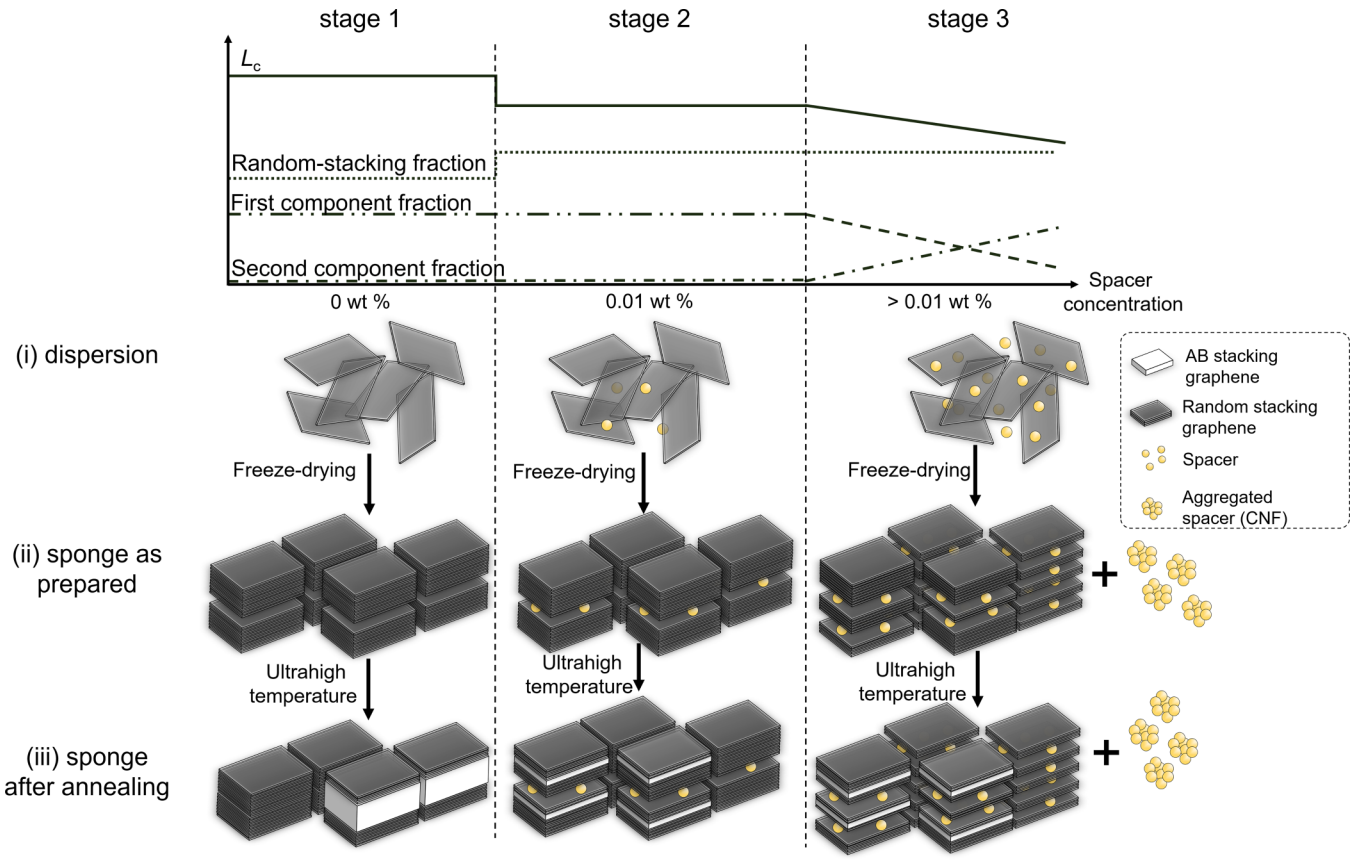

FIG. 7. Schematic image showing the nanospacer effect. The trends in L_c, random-stacking fraction T, and the first and the second component fractions vs the spacer concentration are indicated at the top of the panel. The solid curve donates the L_c. The dotted curve donates the random-stacking fraction. The dash-dot-dotted curve and dash-dotted curve donate the first- and second component fractions, respectively. The mechanism diagram is located below the curve graph. It is divided into three stages from left to right: a graphene sponge without spacers, one with a 0.01 wt. % spacer concentration, and one with a higher spacer concentration, respectively. Each stage is further divided into three steps of the sample preparation process from top to bottom: (i) dispersion after mixing, (ii) the GO sponge after freeze-drying, and (iii) the rGO sponge after the thermal treatment, respectively. For high spacer concentrations, the CNF was aggregated, whereas the ND was not largely aggregated.

This was due to the further stacking of the GO flakes, having about 15 layers at step (ii) that compose the GO sponge, into the rGO, having about 28 layers, during the ultrahigh temperature process at step (iii). Thus, the formation of AB stacking cannot be prevented in the internal region of thick graphene where ethanol-derived species[23,25] cannot access, resulting in a relatively low T value. In the second stage (Fig. 7, middle), a small amount of ND and CNF was added as a spacer at step (i). L_c was reduced to 5.29 and 6.31 nm for CNF and ND, respectively. This was because the added spacers prevented the stacking increase during the thermal process of step (iii) and produced the first component, which is thinner than the ones without spacers. This is also supported by the preservation of the characteristic layer numbers before and after the thermal treatment for the spacer-inserted samples. Due to the very thin layer (∼15) of the first components, the ethanol-derived species can access the surfaces of each graphene flake, resulting in the formation of random-stacking graphene. Actually, according to the G′-band analysis on the Raman spectra, the T value increased to 85% and 89% for CNF and ND, respectively. In the third stage (Fig. 7, right), with an increase in spacer concentration at step (i), the T value did not vary from that of the second stage and remained almost constant. However, L_c gradually decreased at step (iii). The two-component analysis of XRD indicated that the formation of the first component was restrained, while the second one began to form. The second component fraction was increased, resulting in the decrease of L_c. Since the ethanol-derived species can access the internal region of ∼3 nm-thick multilayer graphene (GO) on a substrate,[62,63] and the accessible length becomes double (∼6 nm) for the substrate-free sponges. Accordingly, the T value for the GC and GD samples did not change significantly, because the whole part of these samples, in which the thickness of the first and second components is not more than 6 nm, is within the accessible region for the ethanol-derived species.

4. CONCLUSION

The bulk-scale multilayer graphene sponge with ND or CNF spacers was obtained by freeze-drying and an ethanol-associated thermal treatment. Raman spectroscopy indicated a sudden increase in the random-stacking fraction by the addition of the spacers. According to the XRD analysis, the composite GO/spacer sponges before the thermal treatment possessed characteristic layer numbers comparable to those of the composite rGO/spacer sponges after the treatment, while the layer number of the pure rGO sponge was twice as large as that of the pure GO sponge. As a result, the accessible region for the ethanol-derived species of multilayer graphene increased after adding the spacers. Consequently, the random-stacking fraction increased compared to the pure rGO sponge. The two-component analysis of XRD revealed that the graphene component with a smaller crystalline size was increased with increasing the spacer concentration, indicating that spacers can restrain the formation of the relatively thick component. Compared to the CNF-incorporated samples, the ND-incorporated ones showed a lower fraction of the thick component, indicating the effectiveness of ND as a spacer. Some particles were observed in the SEM image of the sample with a high CNF concentration, indicating that CNFs agglomerated in a high concentration and were unable to act as a spacer. The results proved that inserting nanospacers, especially NDs with high concentrations, can effectively reduce the stacking order in multilayer graphene. The controlled formation of 2D/1D and 2D/0D mixed-dimensional heterostructures is expected to preserve the superior properties of single-layer graphene in bulk scale, such as electric conductivity and flexibility. These practically available properties will pave the way for macroscopic applications, for example, electrode materials in battery[7,8] and supercapacitor,[10,11] and piezoresistive sensor[9,12] for wearable devices.

SUPPLEMENTARY MATERIAL

See the supplementary material for G′-band fitting of the GC samples (Fig. S1), G′-band fitting of the GD samples (Fig. S2), G′-band fitting of the G-1800-Ar (Fig. S3), deconvolution of the 002 peaks of GC-3 and GC-4 (Fig. S4) and GD-3 and GD-4 (Fig. S5) into two components, residential error in XRD peak analysis of the samples with different spacer weight percentages of CNF or ND (Fig. S6), SEM images of the GC samples with different magnification (Fig. S7), and SEM images of the GD samples with different magnification (Fig. S8).

ACKNOWLEDGMENTS

The authors would like to thank Mr. T. Mikazuki and DKS Co. for providing the cellulose nanofiber samples, and Mr. M. Arifuku and Nippon Kayaku Co. for providing the nanodiamond samples. A part of this work was supported by JSPS KAKENHI (Grant Nos. JP15H05867, JP17H02745, JP19H04545, and JP21H01763), JST CREST (No. JPMJCR18R3), Tanikawa Fund Promotion of Thermal Technology, and the Murata Science Foundation. The SEM observation was performed at the Photonics Center, Osaka University. The XRD measurement was conducted at the Comprehensive Analysis Center, ISIR, and Nanotechnology Open Facilities, NOF, Osaka University.

AUTHOR DECLARATIONS

Conflict of Interest

The authors have no conflicts to disclose.

Author Contributions

Zizhao Xu: Conceptualization (equal); Investigation (equal); Visualization (equal); Writing – original draft (equal). **Taiki Inoue:** Writing – review & editing (equal). **Yuta Nishina:** Resources (lead). **Yoshihiro Kobayashi:** Conceptualization (equal); Funding acquisition (equal); Project administration (equal); Supervision (equal); Writing – review & editing (equal).

DATA AVAILABILITY

The data that support the findings of this study are available from the corresponding authors upon reasonable request.

REFERENCES

[1]A. Ambrosi, C. K. Chua, N. M. Latiff, A. H. Loo, C. H. A. Wong, A. Y. S. Eng, A. Bonanni, and M. Pumera, Chem. Soc. Rev. **45**, 2458–2493 (2016).

[2]R. R. Nair, P. Blake, A. N. Grigorenko, K. S. Novoselov, T. J. Booth, T. Stauber, N. M. R. Peres, and A. K. Geim, Science **320**, 1308 (2008).
[3]A. A. Balandin, S. Ghosh, W. Bao, I. Calizo, D. Teweldebrhan, F. Miao, and C. N. Lau, Nano Lett. **8**, 902–907 (2008).
[4]C. Lee, X. Wei, J. W. Kysar, and J. Hone, Science **321**, 385–388 (2008).
[5]D. X. Luong, K. V. Bets, W. A. Algozeeb, M. G. Stanford, C. Kittrell, W. Chen, R. V. Salvatierra, M. Ren, E. A. McHugh, P. A. Advincula, Z. Wang, M. Bhatt, H. Guo, V. Mancevski, R. Shahsavari, B. I. Yakobson, and J. M. Tour, Nature **577**, 647–651 (2020).
[6]Y. Zhang, L. Zhang, and C. Zhou, Acc. Chem. Res. **46**, 2329–2339 (2013).
[7]W. Chen, X. Zhang, L. Mi, C. Liu, J. Zhang, S. Cui, X. Feng, Y. Cao, and C. Shen, Adv. Mater. **31**, 1806664 (2019).
[8]X. Yu, B. Lu, and Z. Xu, Adv. Mater. **26**, 1044–1051 (2014).
[9]H.-Y. Mi, X. Jing, A. L. Politowicz, E. Chen, H.-X. Huang, and L.-S. Turng, Carbon **132**, 199–209 (2018).
[10]X.-N. Tang, C.-Z. Liu, X.-R. Chen, Y.-Q. Deng, X.-H. Chen, J.-J. Shao, and Q.-H. Yang, Carbon **146**, 147–154 (2019).
[11]P. Xu, Q. Gao, L. Ma, Z. Li, H. Zhang, H. Xiao, X. Liang, T. Zhang, X. Tian, and C. Liu, Carbon **149**, 452–461 (2019).
[12]H. Liu, M. Dong, W. Huang, J. Gao, K. Dai, J. Guo, G. Zheng, C. Liu, C. Shen, and Z. Guo, J. Mater. Chem. C **5**, 73–83 (2017).
[13]N. Yousefi, X. Lu, M. Elimelech, and N. Tufenkji, Nat. Nanotechnol. **14**, 107–119 (2019).
[14]V. Chabot, D. Higgins, A. Yu, X. Xiao, Z. Chen, and J. Zhang, Energy Environ. Sci. **7**, 1564 (2014).
[15]F. Li, X. Jiang, J. Zhao, and S. Zhang, Nano Energy **16**, 488–515 (2015).
[16]X. Chen, X. Deng, N. Y. Kim, Y. Wang, Y. Huang, L. Peng, M. Huang, X. Zhang, X. Chen, D. Luo, B. Wang, X. Wu, Y. Ma, Z. Lee, and R. S. Ruoff, Carbon **132**, 294–303 (2018).
[17]L. Liu, H. Zhou, R. Cheng, W. J. Yu, Y. Liu, Y. Chen, J. Shaw, X. Zhong, Y. Huang, and X. Duan, ACS Nano **6**, 8241–8249 (2012).
[18]S. Latil, V. Meunier, and L. Henrard, Phys. Rev. B **76**, 201402 (2007).
[19]H. Peng, N. B. M. Schroter, J. Yin, H. Wang, T.-F. Chung, H. Yang, S. Ekahana, Z. Liu, J. Jiang, L. Yang, T. Zhang, C. Chen, H. Ni, A. Barinov, Y. P. Chen, Z. Liu, H. Peng, and Y. Chen, Adv. Mater. **29**, 1606741 (2017).
[20]K. Uemura, T. Ikuta, and K. Maehashi, Jpn. J. Appl. Phys. **57**, 030311 (2018).
[21]M. Brzhezinskaya, O. Kononenko, V. Matveev, A. Zotov, I. I. Khodos, V. Levashov, V. Volkov, S. I. Bozhko, S. V. Chekmazov, and D. Roshchupkin, ACS Nano **15**, 12358–12366 (2021).
[22]N. Richter, Y. R. Hernandez, S. Schweitzer, J.-S. Kim, A. K. Patra, J. Englert, I. Lieberwirth, A. Liscio, V. Palermo, X. Feng, A. Hirsch, K. Müllen, and M. Kläui, Phys. Rev. Appl. **7**, 024022 (2017).
[23]T. Ishida, Y. Miyata, Y. Shinoda, and Y. Kobayashi, Appl. Phys. Express **9**, 025103 (2016).
[24]R. Negishi, M. Akabori, T. Ito, Y. Watanabe, and Y. Kobayashi, Sci. Rep. **6**, 28936 (2016).
[25]Z. Xu, S. Nakamura, T. Inoue, Y. Nishina, and Y. Kobayashi, Carbon **185**, 368–375 (2021).
[26]Z. Tang, W. Li, X. Lin, H. Xiao, Q. Miao, L. Huang, L. Chen, and H. Wu, Polymers **9**, 421 (2017).
[27]M. Sevilla and A. B. Fuertes, Chem. Phys. Lett. **490**, 63–68 (2010).
[28]D. Jariwala, T. J. Marks, and M. C. Hersam, Nat. Mater. **16**, 170–181 (2017).
[29]X. Sun, Y. Ding, B. Zhang, R. Huang, and D. S. Su, Chem. Commun. **51**, 9145–9148 (2015).
[30]V. Petrakova, V. Benson, M. Buncek, A. Fiserova, M. Ledvina, J. Stursa, P. Cigler, and M. Nesladek, Nanoscale **8**, 12002–12012 (2016).
[31]P. Karami, S. Salkhi Khasraghi, M. Hashemi, S. Rabiei, and A. Shojaei, Adv. Colloid Interface Sci. **269**, 122–151 (2019).
[32]S. Osswald, G. Yushin, V. Mochalin, S. O. Kucheyev, and Y. Gogotsi, J. Am. Chem. Soc. **128**, 11635–11642 (2006).
[33]O. Shenderova, A. Koscheev, N. Zaripov, I. Petrov, Y. Skryabin, P. Detkov, S. Turner, and G. Van Tendeloo, J. Phys. Chem. C **115**, 9827–9837 (2011).
[34]I. I. Kulakova, Phys. Solid State **46**, 636–643 (2004).
[35]X. Duan, Z. Ao, H. Zhang, M. Saunders, H. Sun, Z. Shao, and S. Wang, Appl. Catal. B: Environ. **222**, 176–181 (2018).
[36]M. Zeiger, N. Jäckel, V. N. Mochalin, and V. Presser, J. Mater. Chem. A **4**, 3172–3196 (2016).
[37]N. Morimoto, T. Kubo, and Y. Nishina, Sci. Rep. **6**, 21715 (2016).
[38]L. G. Cançado, K. Takai, T. Enoki, M. Endo, Y. A. Kim, H. Mizusaki, N. L. Speziali, A. Jorio, and M. A. Pimenta, Carbon **46**, 272–275 (2008).
[39]L. M. Malard, M. A. Pimenta, G. Dresselhaus, and M. S. Dresselhaus, Phys. Rep. **473**, 51–87 (2009).
[40]A. C. Gadelha, D. A. A. Ohlberg, C. Rabelo, E. G. S. Neto, T. L. Vasconcelos, J. L. Campos, J. S. Lemos, V. Ornelas, D. Miranda, R. Nadas, F. C. Santana, K. Watanabe, T. Taniguchi, B. van Troeye, M. Lamparski, V. Meunier, V.-H. Nguyen, D. Paszko, J.-C. Charlier, L. C. Campos, L. G. Cançado, G. Medeiros-Ribeiro, and A. Jorio, Nature **590**, 405–409 (2021).
[41]A. C. Ferrari and D. M. Basko, Nat. Nanotechnol. **8**, 235–246 (2013).
[42]A. C. Ferrari, J. C. Meyer, V. Scardaci, C. Casiraghi, M. Lazzeri, F. Mauri, S. Piscanec, D. Jiang, K. S. Novoselov, S. Roth, and A. K. Geim, Phys. Rev. Lett. **97**, 187401 (2006).
[43]T. A. Nguyen, J.-U. Lee, D. Yoon, and H. Cheong, Sci. Rep. **4**, 4630 (2015).
[44]K. F. Mak, J. Shan, and T. F. Heinz, Phys. Rev. Lett. **104**, 176404 (2010).
[45]S. Stankovich, D. A. Dikin, R. D. Piner, K. A. Kohlhaas, A. Kleinhammes, Y. Jia, Y. Wu, S. T. Nguyen, and R. S. Ruoff, Carbon **45**, 1558–1565 (2007).
[46]L. G. Cancado, A. Jorio, E. H. M. Ferreira, F. Stavale, C. A. Achete, R. B. Capaz, M. V. O. Moutinho, A. Lombardo, T. S. Kulmala, and A. C. Ferrari, Nano Lett. **11**, 3190–3196 (2011).
[47]S. Eigler, C. Dotzer, and A. Hirsch, Carbon **50**, 3666–3673 (2012).
[48]B. Ma, R. D. Rodriguez, A. Ruban, S. Pavlov, and E. Sheremet, Phys. Chem. Chem. Phys. **21**, 10125–10134 (2019).
[49]E. B. Barros, N. S. Demir, A. G. Souza Filho, J. Mendes Filho, A. Jorio, G. Dresselhaus, and M. S. Dresselhaus, Phys. Rev. B **71**, 165422 (2005).
[50]A. Mohapatra, M. S. R. Rao, and M. Jaiswal, Carbon **201**, 120–128 (2023).
[51]M. A. Pimenta, G. Dresselhaus, M. S. Dresselhaus, L. G. Cancado, A. Jorio, and R. Saito, Phys. Chem. Chem. Phys. **9**, 1276–1290 (2007).
[52]R. Negishi, C. Wei, Y. Yao, Y. Ogawa, M. Akabori, Y. Kanai, K. Matsumoto, Y. Taniyasu, and Y. Kobayashi, Phys. Status Solidi B **257**, 1900437 (2020).
[53]S. H. Huh, Carbon **78**, 617–621 (2014).
[54]C. Hontoria-Lucas, A. J. López-Peinado, J. D. López-González, M. L. Rojas-Cervantes, and R. M. Martín-Aranda, Carbon **33**, 1585–1592 (1995).
[55]H. He, J. Klinowski, M. Forster, and A. Lerf, Chem. Phys. Lett. **287**, 53–56 (1998).
[56]I. K. Moon, J. Lee, R. S. Ruoff, and H. Lee, Nat. Commun. **1**, 73 (2010).
[57]H. Fujimoto, Carbon **41**, 1585–1592 (2003).
[58]V. Uvarov and I. Popov, Mater. Charact. **58**, 883–891 (2007).
[59]N. Gupta, S. Walia, U. Mogera, and G. U. Kulkarni, J. Phys. Chem. Lett. **11**, 2797–2803 (2020).
[60]J. S. Roh, T. H. Choi, T. H. Lee, H. W. Yoon, J. Kim, H. W. Kim, and H. B. Park, J. Phys. Chem. Lett. **10**, 7725–7731 (2019).
[61]Z. Fan, K. Wang, T. Wei, J. Yan, L. Song, and B. Shao, Carbon **48**, 1686–1689 (2010).
[62]X. He, L. Feng, Z. Zhang, X. Hou, X. Ye, Q. Song, Y. Yang, G. Suo, L. Zhang, Q.-G. Fu, and H. Li, ACS Nano **15**, 2880–2892 (2021).
[63]K. Kanishka, H. De Silva, H.-H. Huang, S. Suzuki, and M. Yoshimura, Jpn. J. Appl. Phys. **58**, SIIB07 (2019).

SUPPLEMENTARY MATERIAL

Stacking Order Reduction in Multilayer Graphene by Inserting Nanospacers

Zizhao Xu[a*], Taiki Inoue[a], Yuta Nishina[b], Yoshihiro Kobayashi[a*]

[a] Department of Applied Physics, Graduate School of Engineering, Osaka University, 2-1 Yamadaoka, Suita, Osaka, 565-0871, Japan

[b] Research Core for Interdisciplinary Sciences, Okayama University, 3-1-1 Tsushima-naka, Kita-ku, Okayama, 700-8530, Japan

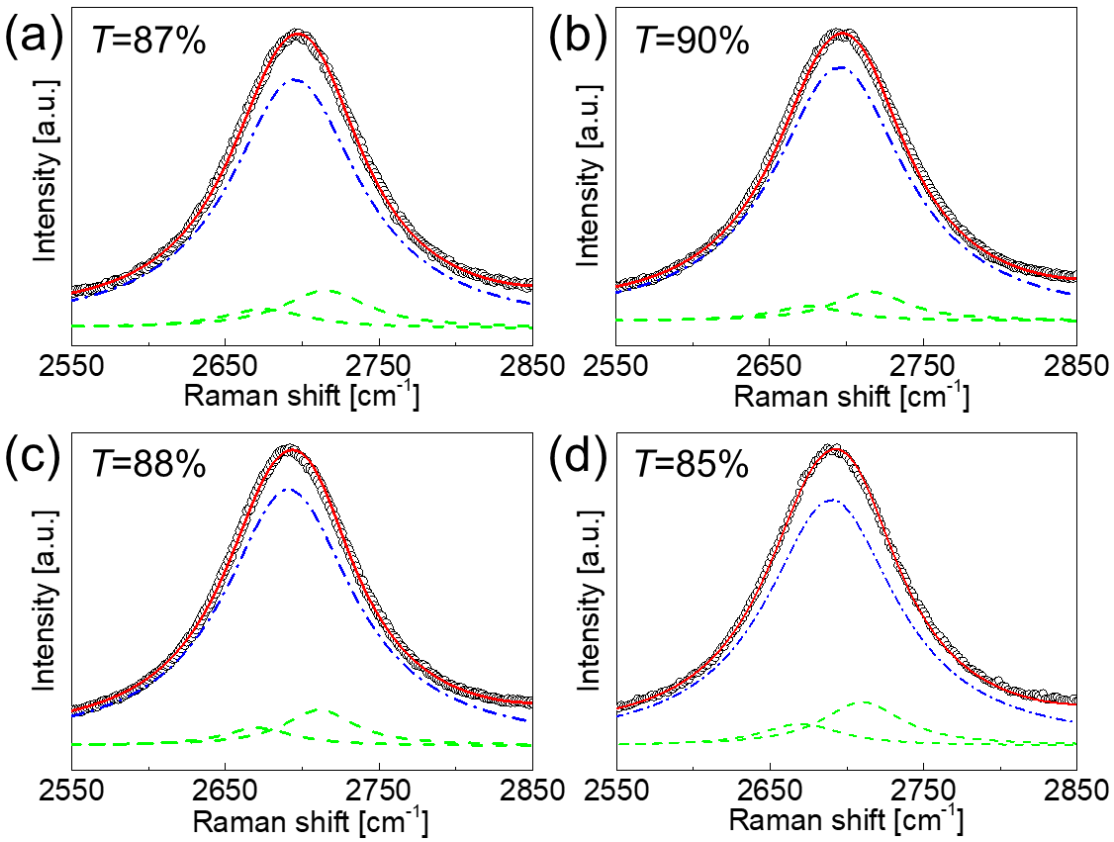

Fig. S1 G′-band fitting of (a) GC-1, (b) GC-2, (c) GC-3, and (d) GC-4, which provides a randomly stacked structure ratio, *T*. Black open circles denote the measured spectra. Blue dashed-dotted curves denote the G'_{2D} components originating from the randomly stacked structure of graphene, while the two green dashed curves denote the G'_{3DA} and G'_{3DB} components derived from the AB-stacked structure. Red solid curves are the sum of the blue and green curves.

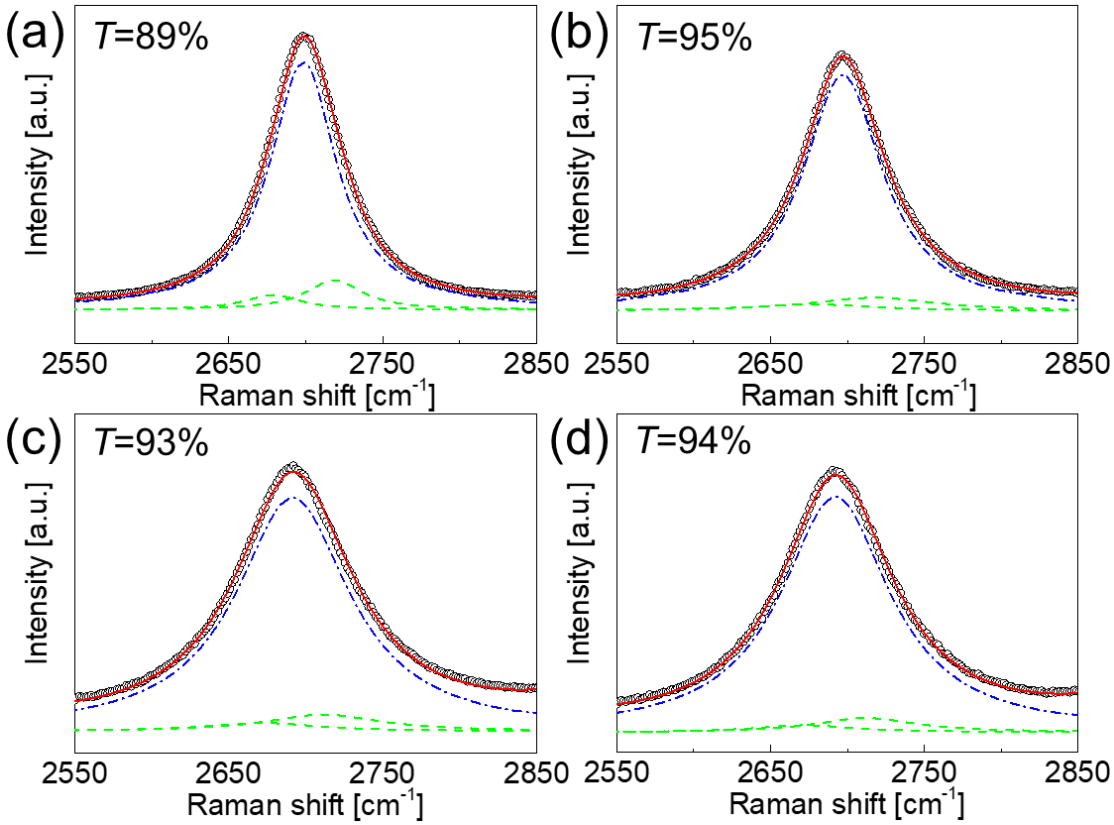

Fig. S2 G′-band fitting of (a) GD-1, (b) GD-2, (c) GD-3, and (d) GD-4, which provides randomly stacked structure ratio, *T*. Black open circles denote the measured spectra. Blue dashed-dotted curves denote the G'_{2D} components originating from the randomly stacked structure of graphene, while the two green dashed curves denote the G'_{3DA} and G'_{3DB} components derived from the AB-stacked structure. Red solid curves are the sum of the blue and green curves.

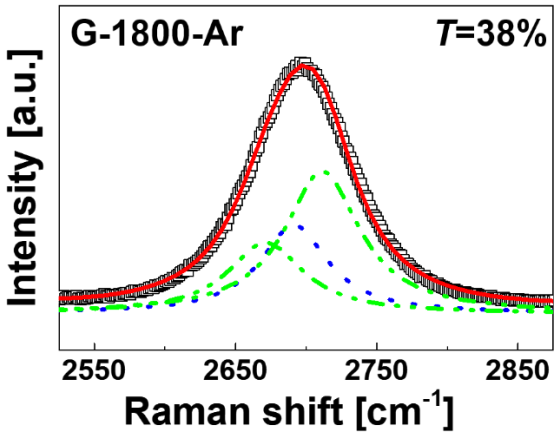

Fig. S3 G′-band fitting of G-1800-Ar[1], which provides randomly stacked structure ratio, *T*. Black open square denotes the measured spectra. Blue dotted curves denote the G'_{2D} components originating from the randomly stacked structure of graphene, while the two green dashed-dotted-dotted curves denote the G'_{3DA} and G'_{3DB} components derived from the AB-stacked structure. Red

solid curves are the sum of the blue and green curves.

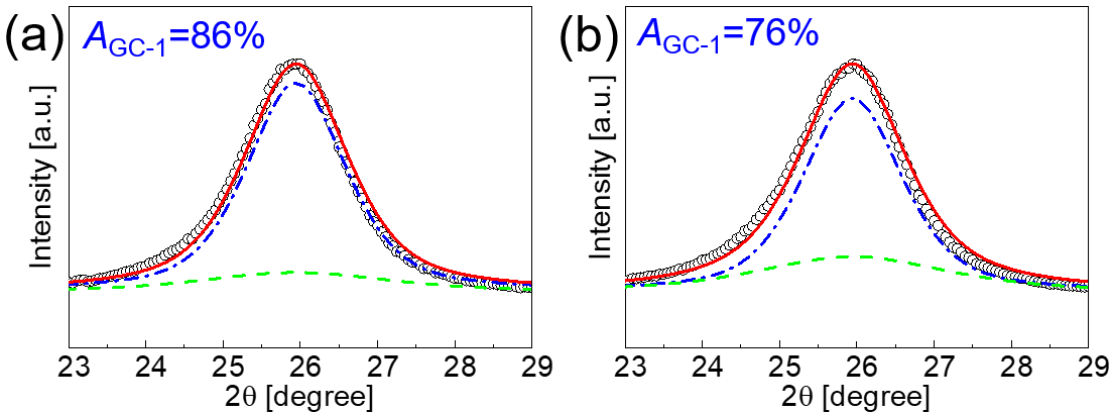

Fig. S4 Deconvolution of the 002 peaks of (a) GC-3 and (b) GC-4 into two components. Black open circles denote the measured XRD patterns. Blue dashed-dotted curves denote the first components originating from the stacked structure of graphene possessing the same d_{002} and L_c as GC-1, while the green dashed curves denote the second components derived from the stacked structure of graphene possessing the same d_{002} as GC-1 but smaller L_c. Red solid curves are the sum of the blue and green curves. Ratios of the first component areas over the total peak area, $A_{GC-1,}$ are displayed.

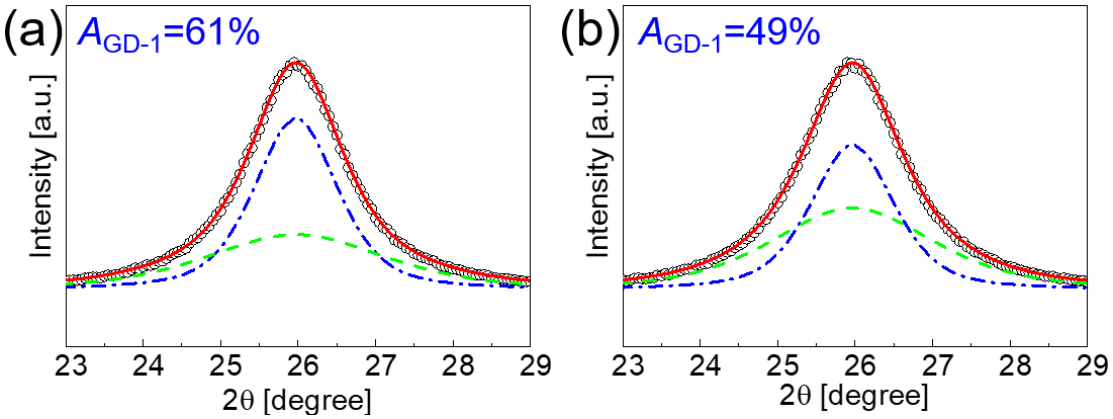

Fig. S5 Deconvolution of the 002 peaks of (a) GD-3 and (b) GD-4 into two components. Black open circles denote the measured XRD patterns. Blue dashed-dotted curves denote the first components originating from the stacked structure of graphene possessing the same d_{002} and L_c as GD-1, while the green dashed curves denote the second components derived from the stacked structure of graphene possessing the same d_{002} as GC-1 but smaller L_c. Red solid curves are the sum of the blue and green curves. Ratios of the first component areas over the total peak area, $A_{GC-1,}$ are displayed.

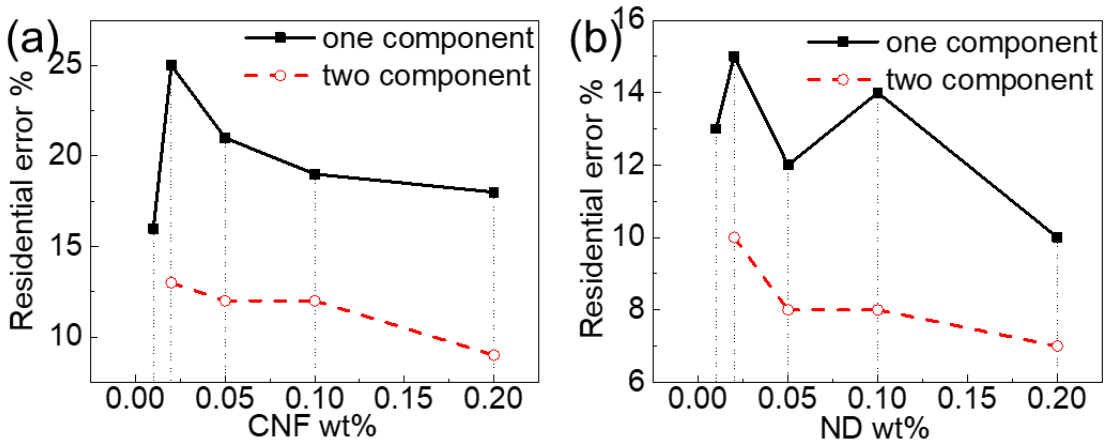

Fig. S6 Residential error in XRD peak analysis of samples with different spacer weight percentages of (a) CNF and (b) ND. Black-filled squares with solid lines denote the residential error of one component fitting, while the red open circles with dash lines denote the residential error of two components fitting.

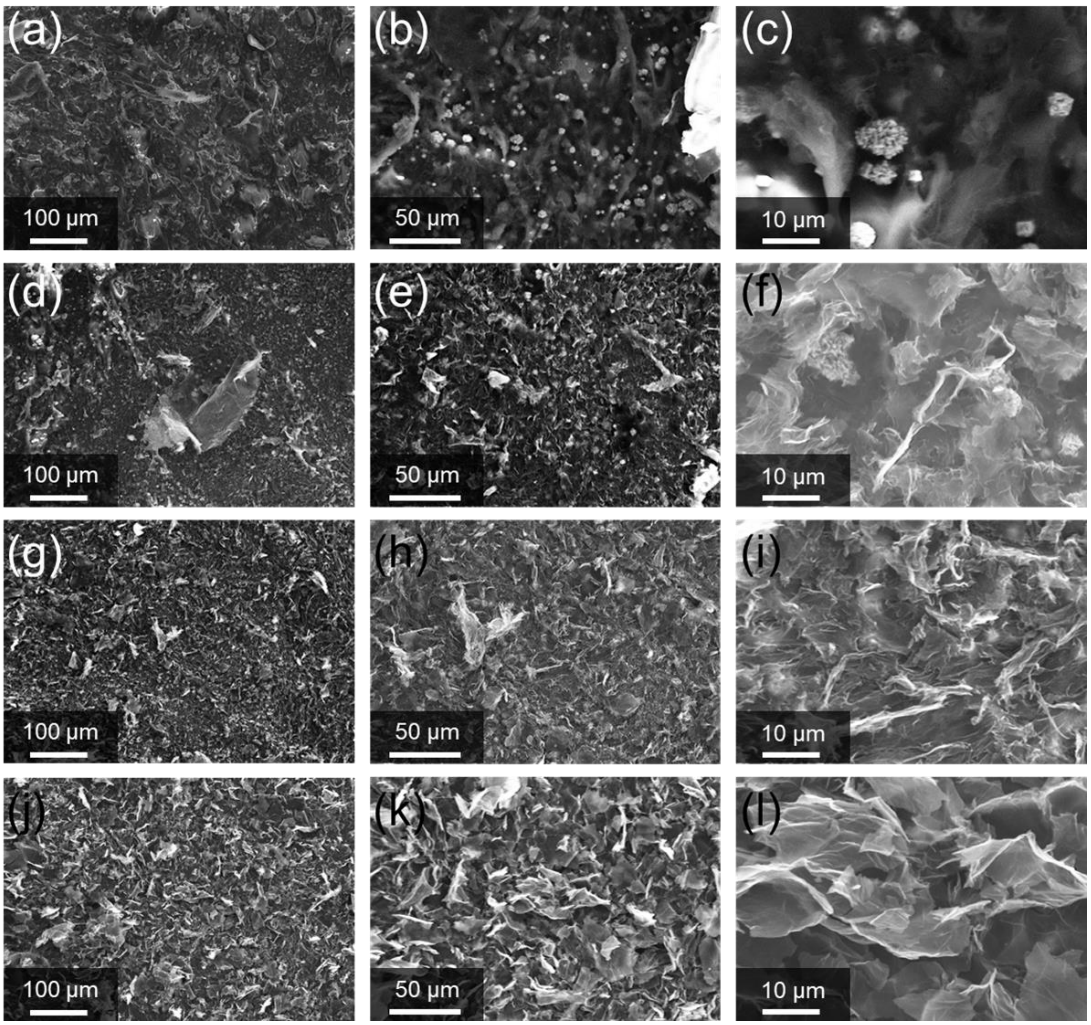

Fig. S7 SEM images of (a-c) GC-5, (d-f) GC-3, (g-i) GC-1, and (j-l) G-0 with different

magnification.

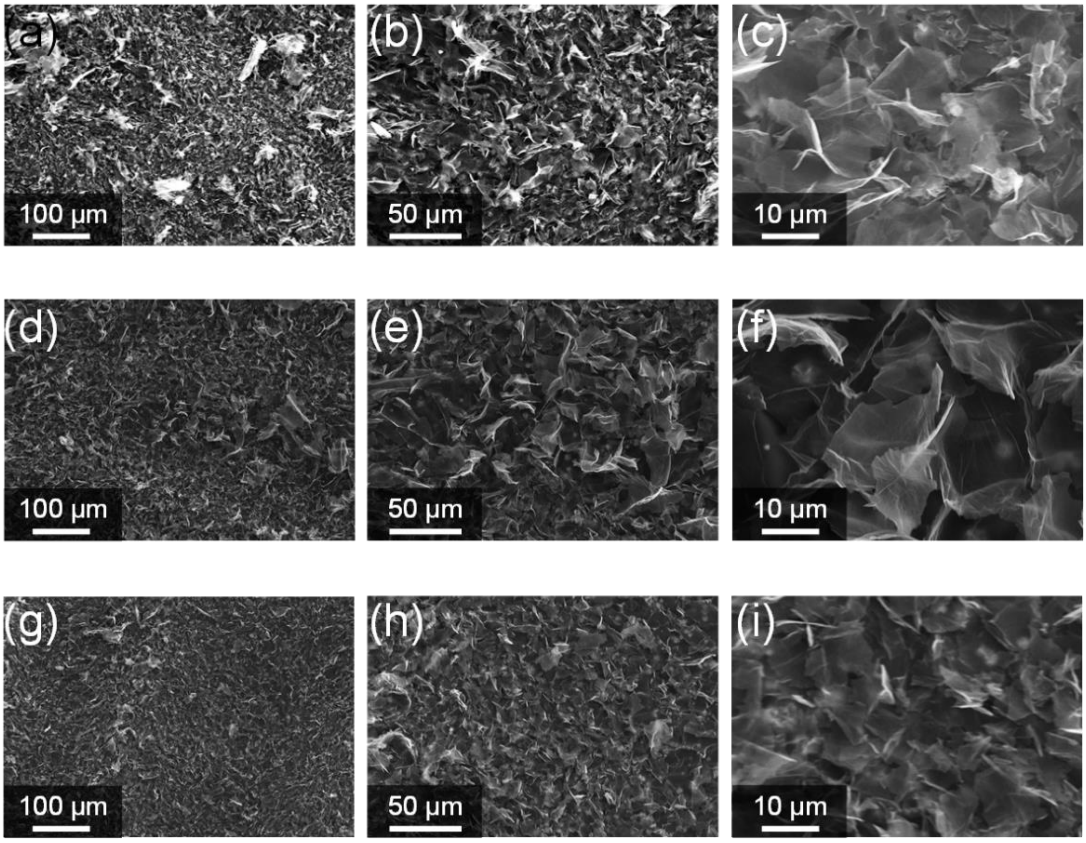

Fig. S8 SEM images of (a-c) GD-5, (d-f) GD-3, and (g-i) GD-1 with different magnification.

Renference

[1] Z. Xu, S. Nakamura, T. Inoue, Y. Nishina, and Y. Kobayashi, Carbon **185,** 368 (2021).